

PERFORMANCE OF RSM TURBULENCE MODEL IN PREDICTING THE AIRFLOW IN A VENTILATED ROOM

Rafael Elias Mazzaro, rafael.mazzaro@consultant.volvo.com

Viviana Cocco Mariani, viviana.mariani@pucpr.br

Kátia Cordeiro Mendonça, k.mendonca@pucpr.br

Department of Mechanical Engineering
Pontifícia Universidade Católica do Paraná – PUCPR
Rua Imaculada Conceição, 1155, 80215-901, Curitiba – PR - Brazil

Abstract. *The objective of the present study is to analyze numerically the turbulent airflow in a room ventilated by an isotherm horizontal wall jet, obtaining data to project more efficient ventilation systems. The experimental data from Annex 20 test cell, which represents a large rectangular room where the air is supplied horizontally by a rectangular opening on the top of left wall and is exhausted through another rectangular opening on the bottom of right wall, were used to check the numerical results. The airflow is characterized by Reynolds number based on the height of the air inlet. The governing equations have been solved using the volume finite method and the turbulence has been modeled by a Reynolds-Stress Model, which is a model of second moment closure. In order to evaluate the influence of the aspect ratio of the room and the width of the inlet slot on the prediction of the indoor airflow, results for Reynolds number of 5,000 are presented for two geometric aspect ratios, one corresponding to a room as large as high and the other to a room 4.7 times larger than high, considering two inlet arrangements. On the whole, the predictions in terms of velocity profiles by the RSM tested are similar to those from the standard $k-\varepsilon$ model, while the streamlines estimates more recirculations than the latter. Concerning the changes in the aspect ratio of the room and in the inlet slot width, both affect the air movement inside the room strongly.*

Keywords: *Reynolds Stress Model, standard $k-\varepsilon$ model, turbulence, indoor airflow, horizontal jet.*

1. INTRODUCTION

The number of people working in closed environments has increased in recent decades, culminating today in a significant population number working in that condition. Due to this fact, several studies are being conducted improving work conditions in these environments. Most of them have indoor air-conditioning systems to maintain temperature and humidity controlled, providing a comfortable situation for workers. Note that this feeling of thermal comfort experienced by the user is dependent on several factors such as temperature and humidity, but even in a room with appropriate temperature and humidity, the user can be subject to a state of thermal discomfort due to the possible existence of high gradients of temperature and velocity on the environment, or a situation where the air jet produced by the air conditioner reaches the user at a high flow rate.

Thus, air-conditioning systems can produce gradients of the psychrometric properties and, as a consequence: a) cause to occupants a sensation of discomfort even when their global thermal perceptions of the indoor environment remain satisfactory; b) expose the occupants differently to pollutants sources and c) affect the heat and mass transfer between the indoor environment and its envelope and therefore the building energy consumption. Hence, for accurately evaluating the energy consumption in conditioned spaces while maintaining thermal comfort and healthy conditions, it is important to take into account the indoor air distribution on the evaluation.

Accurate simulation of flow in enclosed environments is essential to improve and optimize ventilation systems and to save energy. In addition, different airflow patterns can lead to very different heat transfer coefficients and temperature distributions in confined spaces. The corresponding heat and loss will not be the same. The Computational Fluid Dynamic (CFD) simulations often use turbulence models, since most indoor flows are turbulent. Numerical and experimental studies about turbulent flow are described quickly afterwards.

Nielsen *et al.* (1978) performed experimental and numerical simulations of jet airflow inside a room. The experimental measurements were made using laser anemometry of velocity profiles. In the turbulence numerical solution it was used the standard $k-\varepsilon$ model. The results showed that this model is able to describe the mean flow, except in regions of low velocities. Melikov and Nielsen (1989) studied experimentally the comfort conditions in ventilated environments. The results showed the importance of evaluated the temperature gradient and air vertical velocity on the thermal comfort perceived by occupants. The experimental data for non-isothermal and isothermal cases obtained by Nielsen *et al.* (1978) were adopted in the Annex 20 (Nielsen, 1990) like a standard for comparison and validation of computer codes solving airflow in environments. Chen (1996) compared the efficiency of four turbulence models (three Reynolds Stress Models and the standard $k-\varepsilon$ model) to predict numerically the airflow into a room with heat transfer by convection natural, forced, and mixed. The results showed that RSM models perform better than the standard $k-\varepsilon$ model. Although not satisfactorily, the anisotropic RSM models could predict secondary vortex, however they took 50-20 times longer to converge compared to the standard $k-\varepsilon$ model.

Voigt (2000) compared the performance of five turbulence models in predicting, two-dimensionally, the isothermal airflow inside the geometry from Nielsen (1990). The five models tested were standard $k-\varepsilon$, low-Reynolds $k-\varepsilon$, $k-\omega$, $k-\omega$

baseline (BSL) and $k-\omega$ Shear Stress Transport (SST). The results were confronted against the experiments of Nielsen (1990) and showed that the models provided good results compared with the experimental data, the main differences found were attributed to three-dimensional effects.

Schalin and Nielsen (2004) compared the performance of the standard $k-\varepsilon$ and RSM model (models for high Reynolds number). The standard $k-\varepsilon$ model provides acceptable results, but there are problems that require more elaborate models such as RSM. The jet near the wall could be represented in more detail using the wall reflection. Lindner *et al.* (2008) investigated the performance of two eddy viscosity turbulence models in predicting the three-dimensional airflow in a rectangular room whose floor was heated. The performance of the standard $k-\varepsilon$ model for such flows was generally better than that of the $k-\omega$ model. The $k-\omega$ model over-predicted the temperature in the floor. Susin *et al.* (2009) evaluated the influence on the airflow caused by variations of the inlet width using three turbulence models: standard $k-\varepsilon$, RNG $k-\varepsilon$ and $k-\omega$. The authors have found that the predictions from the three models were comparable to the experimental results available in the current literature, with the standard $k-\varepsilon$ consuming less computation time. Variations in the main and second flows due to the variation of the inlet width were verified.

The objective of this study is then to contribute to the improvement of the thermal comfort and indoor air quality of conditioned environments, as well as to the reduction in the energy consumption in buildings through the numerical investigation of the three-dimensional airflow caused by the presence of a horizontal jet in a rectangular room, employing a RSM (Reynolds Stress Model) turbulence model. In particular, this work intends to evaluate the effect of the width of the room and the width of the inlet slot on the prediction of the isothermal airflow inside the Annex 20 cavity (Nielsen, 1990). The choice of a RSM turbulence model is due to precedent studies (Chen 1996, Moureh and Flick 2003, Schälin and Nielsen, 2004) have shown that this kind of model could predict second flows better than two-equation models.

2. MATHEMATICAL MODELING

Reynolds (1894) decomposed the Navier-Stokes equations in two parties, one related to the average value of the velocity vector and another related to its fluctuation, and applied the time average operator on them to study turbulent flows. The resulting set of equations is known as Reynolds Average Navier-Stokes (RANS) equations and gives information about the mean flow. Although this approach is not able to describe the multitude of length scales involved in turbulence, it has been largely used all of the world because in many engineering applications the information about the mean flow is quite satisfactory.

Considering that density and viscosity variations are small so that their effects on turbulence can be ignored, the fluid is Newtonian, the flow is incompressible and the steady state, the governing RANS equations in Cartesian coordinates can be expressed by (Versteeg and Malalasekera, 1995):

$$\frac{\partial U_i}{\partial x_i} = 0, \quad (1)$$

$$\rho \frac{\partial(U_i U_j)}{\partial x_j} = -\frac{\partial P}{\partial x_i} + \frac{\partial}{\partial x_j} \left(\mu \frac{\partial U_i}{\partial x_j} - \overline{\rho u_i u_j} \right) + F_i, \quad (2)$$

where U_i and U_j are components of the average velocity vector [m/s], ρ is the fluid density [kg/m³], μ is the dynamic viscosity of the fluid [Pa.s], P is the mean average pressure [Pa] and F_i is a component of the bulk force vector [N]. The extra-term that appears in Eq. (2) comparing to the original Navier-Stokes equations, $\overline{u_i u_j}$, is the product of fluctuation velocities [m²/s²] termed Reynolds stresses and is never negligible in any turbulent flow. It represents the increase in the diffusion of the mean flow due to the turbulence. Equations (1) and (2) can only be solved if the Reynolds stress tensor are known, a problem referred to as the ‘closure problem’ since the number of unknowns is greater than the number of equations.

The main goal of the turbulence studies based on RANS equations is therefore to determine the Reynolds stresses. According to Kolmogorov (1942) they can be evaluated by the following expression:

$$-\overline{u_i u_j} = \nu_t \left(\frac{\partial U_i}{\partial x_j} + \frac{\partial U_j}{\partial x_i} \right) - \frac{2}{3} \delta_{ij} k, \quad (3)$$

where δ_{ij} is the Kronecker delta and the kinetic energy of the turbulent motion, k , is defined as $k = \overline{u_i u_i} / 2$ [m²/s²]. Substitution of Eq. (3) into Eq. (2) results in the average Navier-Stokes equations with the Reynolds stresses modeled via the viscosity concept,

$$\frac{\partial(U_i U_j)}{\partial x_j} = -\frac{1}{\rho} \frac{\partial P'}{\partial x_i} + \frac{\partial}{\partial x_j} \left[(v + \nu_t) \left(\frac{\partial U_i}{\partial x_j} + \frac{\partial U_j}{\partial x_i} \right) \right] \quad (4)$$

where μ_t is the turbulent viscosity, $P' = P + 2/3k$ is the modified pressure.

The turbulent viscosity can be expressed as the product of a velocity scale, u [m/s], and a length scale, L_μ [m], $\mu_t = \rho u L_\mu$. Considering the velocity scale being calculated by $u = k^{1/2}$, Kolmogorov (1942) and Prandtl (1945) independently proposed the following relation for the turbulent viscosity,

$$\mu_t = \rho c_\mu k^{1/2} L_\mu, \quad (5)$$

where $c_\mu (=0.09)$ is an empiric constant.

In order to complete the set of equations described above, the most popular turbulence models define two other transport equations: one for the turbulent kinetic energy, k , and another for a variable that relates k to L_μ . These models are called two equations models, and the standard k - ε model (Launder and Spalding, 1974) will be employed in this study for comparative purposes.

2.1 Standard k - ε model

Due to its robustness, economy and acceptable results for a considerable amount of flows the standard k - ε model has been the most used model for numerical predictions of industrial flows. However, it is known to have deficiencies in some situations involving streamline curvature, acceleration and separation.

In this model, proposed by (Launder and Spalding, 1974), the second variable for the complementary transport equations is the rate of the viscous dissipation, ε [m^2/s^3], which is related to k by:

$$\varepsilon = k^{3/2} / L. \quad (6)$$

The turbulent viscosity ν_t is calculated in the k - ε model as

$$\nu_t = c_\mu k^2 / \varepsilon. \quad (7)$$

Therefore, the set of equations concerning the standard k - ε model is composed of Eqs. (1) and (4) and two transport equations for k and ε that are, respectively, given by:

$$\rho \frac{\partial(U_j k)}{\partial x_j} = \frac{\partial}{\partial x_j} \left[\left(\mu + \frac{\mu_t}{\sigma_k} \right) \frac{\partial k}{\partial x_j} \right] + \mu_t \left[\frac{\partial U_i}{\partial x_j} + \frac{\partial U_j}{\partial x_i} \right] \left[\frac{\partial U_i}{\partial x_j} \right] - \rho \varepsilon \quad (8)$$

$$\rho \frac{\partial(U_j \varepsilon)}{\partial x_j} = \frac{\partial}{\partial x_j} \left[\left(\mu + \frac{\mu_t}{\sigma_\varepsilon} \right) \frac{\partial \varepsilon}{\partial x_j} \right] + c_1 \mu_t \frac{\varepsilon}{k} \left[\frac{\partial U_i}{\partial x_j} + \frac{\partial U_j}{\partial x_i} \right] \left[\frac{\partial U_i}{\partial x_j} \right] - c_2 \rho \frac{\varepsilon^2}{k} \quad (9)$$

where $c_1 = 1.42$; $c_2 = 1.92$; $\sigma_k = 1$ e $\sigma_\varepsilon = 1.22$ are empirical constants.

As Eqs. (8) and (9) cannot describe correctly the movement of the fluid near solid surfaces, the so called wall-functions are required to make it applicable to the entire domain.

2.2 RMS model

The Reynolds Stress Model (RSM) is based on transport equations of the Reynolds tensor and dissipation rate of turbulent kinetic energy. Solving a transport equation for each component of the Reynolds tensor the RSM add for a three-dimensional flow six new equations to the equations system. The RSM model is called a second moment closure due to model only terms of third or higher order. There are several variations of RSM, the model used in this study is known as RSM-LLR described in Launder *et al.* (1975). The transport equations for the Reynolds tensor are derived from the Navier-Stokes equations and are described by:

$$\rho \frac{\partial(U_j \tau_{ik})}{\partial x_j} = P_{ik} - \rho \varepsilon_{ik} + \frac{\partial}{\partial x_j} \left[\nu \frac{\partial \tau_{ik}}{\partial x_j} + C_{ikj} \right] + \Pi_{ik}, \quad (10)$$

where the first term represents the variation rate of the viscous stress tensor, τ , due to production, P , and dissipation of the turbulent kinetic energy, ε , the fourth term represents the molecular and turbulent diffusion, and the last term correlates pressure and tension.

The production, the dissipation of the turbulent kinetic energy, and the turbulent diffusion can be described by,

$$P_{ik} = - \left[\tau_{ik} \frac{\partial U_k}{\partial x_j} + \tau_{ik} \frac{\partial U_i}{\partial x_j} \right] \quad (11)$$

$$\varepsilon_{ik} = \frac{2}{3} \varepsilon \delta_{ik} \quad (12)$$

$$C_{ikj} = \overline{\rho u_i' u_k' u_j'} + \overline{p' u_i' \delta_{kj}} + \overline{p' u_k' \delta_{ij}} \quad (13)$$

where δ is the Kronecker delta operator. The last term in Eq. (10) combine the pressure with deformation of the flow, this term is responsible by redistribution of turbulent kinetic energy among the components of the Reynolds stress tensor, and can be described as:

$$\Pi_{ik} = \frac{p'}{\rho} \left(\frac{\partial u_i'}{\partial x_k} + \frac{\partial u_k'}{\partial x_i} \right), \quad (14)$$

In the RSM-LLR model used in this study, proposed by Launder *et al.* (1975), the Eq. (14) is:

$$\Pi_{ik} = -\rho \varepsilon C_1 a + C_2 \rho k S + C_4 \rho k (aS^T + Sa^T - 2a \cdot S \delta / 3) + C_5 \rho k (aa + Wa^T)], \quad (15)$$

where $a = u_i / k - 2\delta / 3$ is the anisotropy tensor, $S = [\bar{\nabla} U + (\bar{\nabla} U)^T] / 2$ is the tensor rate, $W = [\bar{\nabla} U - (\bar{\nabla} U)^T] / 2$ is the vorticity, $C_1 = 1.8$, $C_2 = 0.8$, $C_4 = C_5 = 0.6$ are constants.

3. NUMERICAL METHODOLOGY

The numerical solution of the governing equations was performed using the commercial computational fluid dynamics code CFX, version 11.0 (2007). In this code the conservation equations for mass, momentum, and turbulence quantities are solved using the finite volume discretization method generated by unstructured Voronoi Diagram. For this practice the solution domain is divided in small control volumes, using a non-staggered grid scheme, and the governing differential equations are integrated over each control volume with the Gauss' theorem. The resulting discrete linear equations system is solved using an Algebraic Multigrid called Additive Correction accelerated Incomplete Lower Upper (ILU) factorization technique. It is an iterative solver whereby the exact solution of the equations is approached during the course of several iterations.

The spatial discretization (mesh number) was performed using the commercial software ICFM CFD version 11.0. The choice of this software to create the mesh was based on the fact that it provides the division of geometry into blocks, for which one can assign different levels of independent refinement. Blocks were created close to the ceiling, to the floor and in the outlet zone of the airflow, because of the high velocity gradients in these regions. The mesh was created using hexahedral elements, with refinement in the regions near the walls, taking care to ensure the transition between regions occur smoothly.

Three grid levels were tested, the grids with 130,000 (Cases 1 and 2) and 400,000 (Cases 3 and 4) volumes were chosen to simulate the investigated flow using the symmetry of the computational domain. The convergence criteria was calculated using the normalized residual,

$$\tilde{r}_\phi = \frac{r_\phi}{a_p \Delta\phi} < \gamma, \quad (16)$$

where r_ϕ is the raw residual control volume imbalance, a_p is representative of the control volume coefficient, $\Delta\phi$ is a representative range of the variable in the domain, ϕ represent all variables and $\gamma = 10^{-5}$ is the stopping criterion. All meshes were created using the same expansion factor, 1.2, for the regions that were refined.

All computational simulations were performed using a computer AMD Athlon 64X2 Dual Core, Processor 4000 +2.11 Ghz, 3 GB RAM.

4. RESULTS AND DISCUSSIONS

4.1. Problem description

The isothermal airflow regarding the Annex 20 benchmark described in Nielsen (1990), for which some experimental and numerical data are available in the current literature, was chosen to perform the proposed analysis. The measurements were carried out in a rectangular scaled-down room where the air enters horizontally at the top of one side and leaves the room at the bottom of the opposite side through rectangular openings. Figure 1 shows a sketch of this experimental device, as well as the positions (blue and red lines) in which mean velocity profiles were measured.

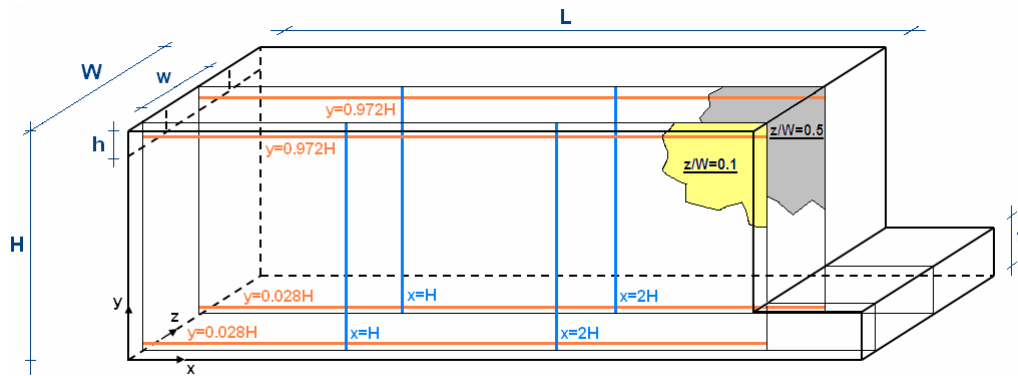


Figure 1. Sketch of the three-dimensional test case.

In this work, the CFD simulations were conducted in the half of the full-scale geometry equivalent to the Annex 20 test cell with the following dimensions: height $H = 3.0$ m, length $L = 3.0H$, width $W = 3.0H$ or $4.7H$, inlet height $h = 0.056H$, outlet height $t = 0.16H$. In these two geometries, two inlet widths were considered: occupying 50% and 100% of the environment width.

The inlet boundary conditions for the velocity components in the x, y and z directions were specified as $U = U_0$ and $V = W = 0$, respectively, with U_0 being the air average velocity in the inlet of the cavity obtained from Reynolds number based on the inlet height, $Re = U_0 h / \nu$, equals to 5,000. Regarding k and ϵ , the inlet boundary conditions were calculated by $k_0 = 1.5(0.04U_0)^2$ and $\epsilon_0 = 10k^{3/2}/h$. Zero relative pressure and zero gradients for the other variables were applied as the boundary conditions for the outlet. At the solid boundaries the no-slip and the impermeable wall boundary conditions were imposed for the velocity components, that are, $U = V = W = 0$. The turbulence quantities k and ϵ are nulls at the walls. All walls were assumed as adiabatic. A summary of the studied cases is described in Table 1.

Table 1 – Configurations studied.

| Case | L/H | W/H | w/W | Re |
|------|-----|-----|-----|-------|
| 1 | 3 | 1 | 1 | 5,000 |
| 2 | 3 | 1 | 0.5 | 5,000 |
| 3 | 3 | 4.7 | 1 | 5,000 |
| 4 | 3 | 4.7 | 0.5 | 5,000 |

4.2. Comparative analyses

In this section, the numerical results obtained from the turbulence models investigated regarding the mean velocities at four positions of the room, $x = H$, $x = 2H$, $y = 0.028H$ and $y = 0.972H$, are presented for the central plane, $z/W = 0.5$, and for the plane $z/W = 0.1$, as well as the streamlines for the planes $x = H$ and $x = 2H$.

Figures 2 and 3 compare the numerical dimensionless mean velocity profiles to the experimental data from Nielsen (1978) and numerical data from Susin *et al.* (2009) for Case 1, whose inlet slot is as large as the room, at $z/W = 0.5$ and $z/W = 0.1$, respectively.

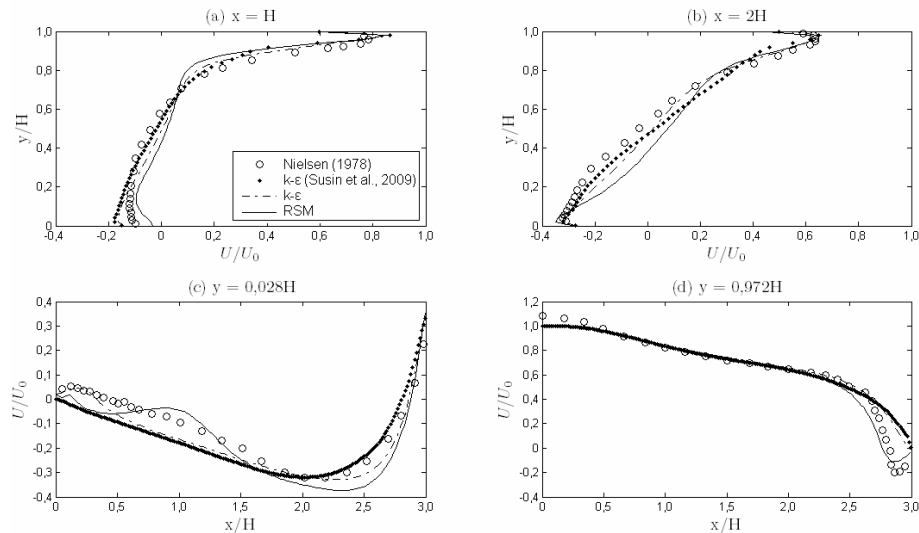


Figure 2. Comparison of dimensionless mean velocity profiles predicted by the investigated turbulence models to the experimental data at plane $z/W = 0.5$, for $W=3H$ and $w/W = 1$ (Case 1).

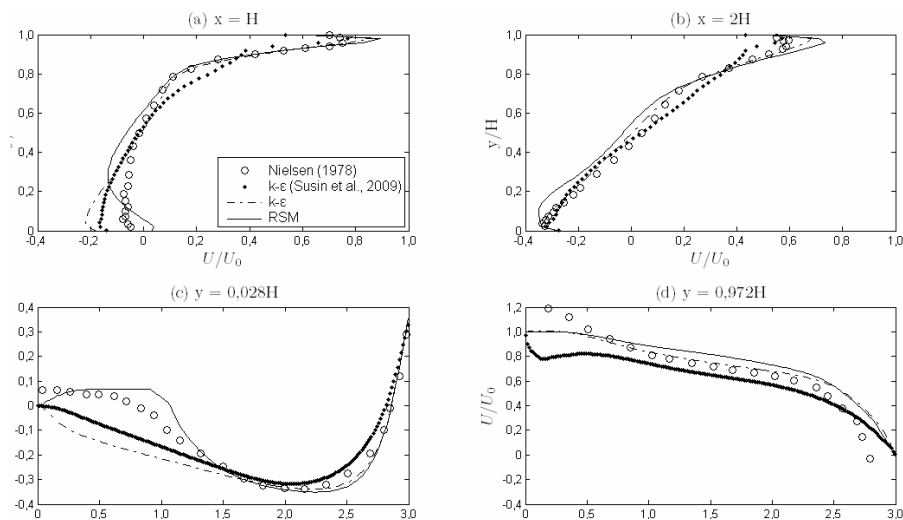


Figure 3. Comparison of dimensionless mean velocity profiles predicted by the investigated turbulence models to the experimental data at plane $z/W = 0.1$ for $W=3H$ and $w/W = 1$ (Case 1).

Observing Fig. 2, one can note that, globally, the standard $k-\epsilon$ model produced results close to those from the experimental set-up and numerical results from Susin *et al.* (2009) where a non-structured grid has been employed. As in Susin *et al.* (2009), the standard $k-\epsilon$ model underestimated the velocity in the region close to the floor although some improvement has been obtained next to the left wall (see Figs. 2a and 2c), and overestimated the velocity in the jet region near the right wall (see Fig. 2d). Concerning the RSM model, Fig. 2d shows that this model was able to predict adequately the jet region, including the portion in the proximity of the right wall that is affected by the jet recirculation generated by this wall. In spite of that, the velocity profiles have been worse represented by this model, probably due to the use of the same grid employed with the standard $k-\epsilon$ model investigated in this work.

In the plane $z/W=0.1$, Fig. 3 shows that the RSM model could describe the behavior of the experimental data better than both simulations obtained with the standard $k-\epsilon$ model in the region next to the floor (see Figs. 3a and 3c). Similar

to the numerical results from Susin *et al.* (2009), in this case the root mean square error was around 7% for both models.

The dimensionless mean velocity profiles obtained for the case whose inlet slot width is half of the width of the room (Case 2) are shown in Fig. 4 for the positions $x = H$ and $x = 2H$, at two planes $z/W = 0.5$ and $z/W = 0.1$. Note that the predictions from the two turbulence models are close to each other, underestimating the velocity values near the ceiling in the jet region, except for the position $x = H$. The root mean square error for both models is inferior to that of Case 1 and about 4%. As indicated by the experimental data, the reduction in the inlet slot width produces a reduction in the mean velocities in the plane $z/W = 0.1$, that is not observed in Case 1 since the airflow can be considered approximately two-dimensional.

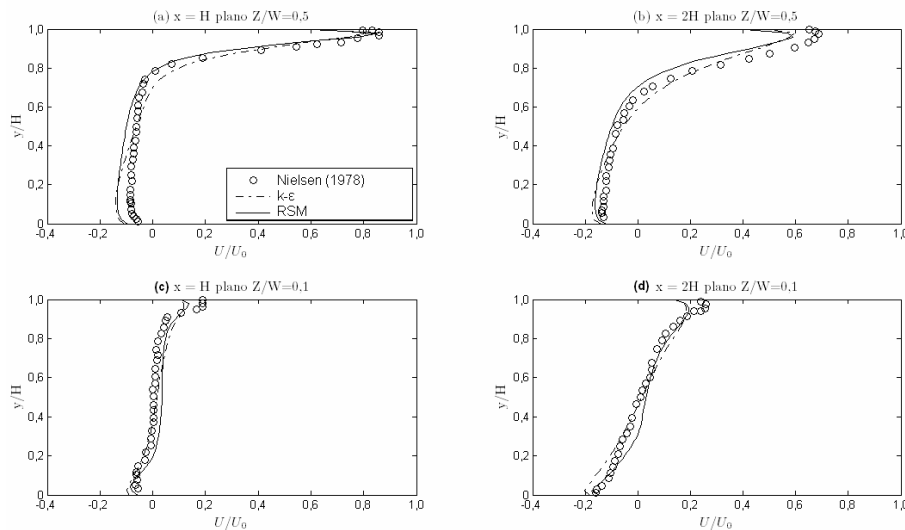


Figure 4. Comparison of dimensionless mean velocity profiles predicted by the investigated turbulence models to the experimental data at planes $z/W = 0.5$ and 0.1 , for $W=3H$ and $w/W = 0.5$ (Case 2).

In spite of the similarities in the velocity profiles predicted by the two models, the comparison between the streamlines at planes $x = H$ and $x = 2H$ for Case 2, illustrated in Fig. 5, shows that the standard $k-\epsilon$ model describes a flow approximately vertical at $x = H$, while the RSM model indicates that, in this plane, the flow is bended to the left on the lower left corner of the room, because of a recirculation in this region. Additionally, in comparison to the standard $k-\epsilon$ model results, the RSM model indicates that the jet width at plane $x = 2H$ is smaller and the main flow is dislocated to the upper left side of the room.

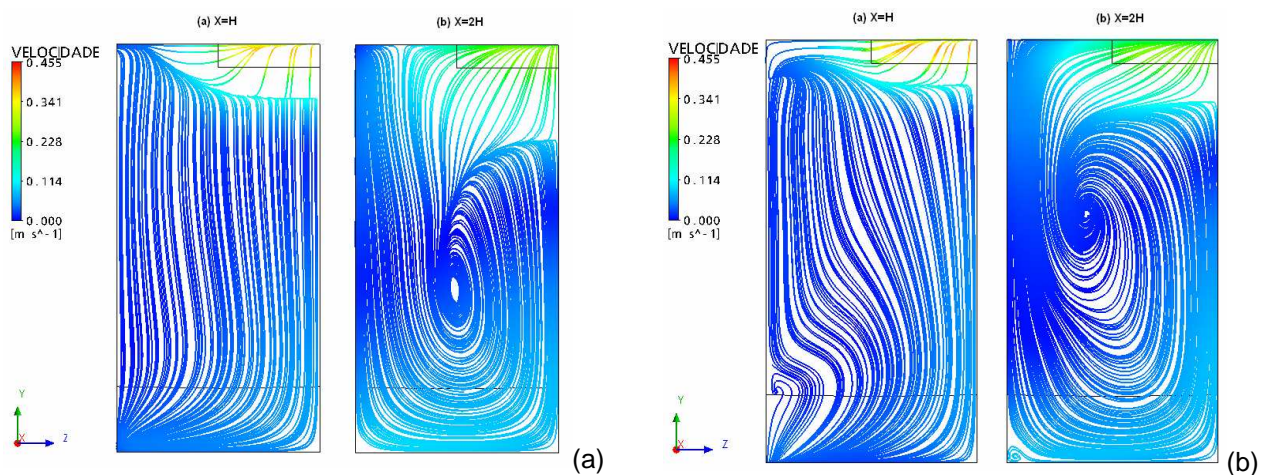


Figure 5. Comparison of streamlines predicted by the (a) standard $k-\epsilon$ and (b) RSM models at planes $x = H$ and $x = 2H$, for $W = 3H$ and $w/W = 0.5$ (Case 2).

In order to evaluate the influence of the room width on the behavior of the flow, the velocity profiles from the RSM and standard $k-\epsilon$ models for Case 3 are compared to those from the RSM model for Case 1 in the planes $z/W = 0.5$ and $z/W = 0.1$, respectively, in Figs. 6 and 7, and the streamlines for the planes $x = H$ and $x = 2H$ are compared in Fig. 8.

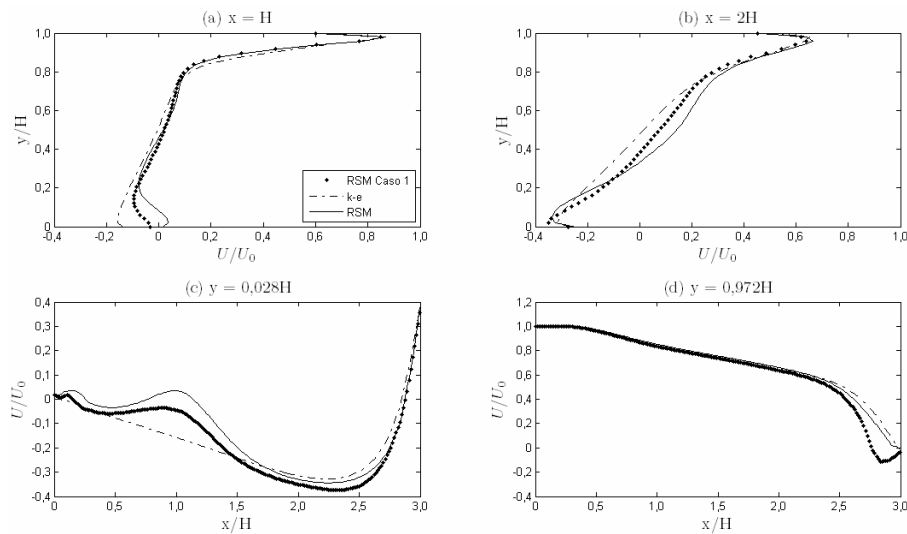


Figure 6. Comparison of dimensionless mean velocity profiles predicted by the standard $k-\varepsilon$ and RSM models for $W = 4.7H$, and $w/W = 1$ (Case 3) to RSM model data for $W = 3H$, and $w/W = 1$ (Case 1) at plane $z/W = 0.5$.

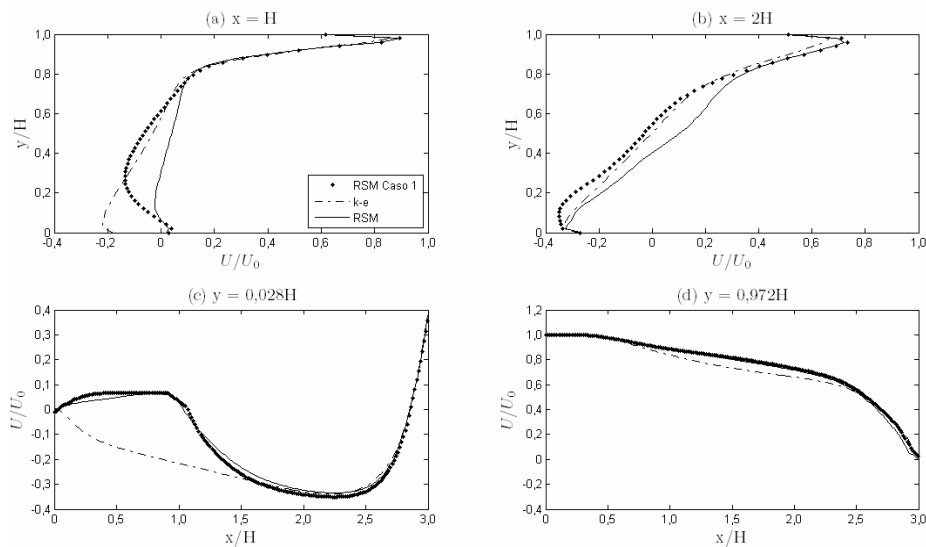


Figure 7. Comparison of dimensionless mean velocity profiles predicted by the standard $k-\varepsilon$ and RSM models for $W = 4.7H$, and $w/W = 1$ (Case 3) to RSM model data for $W = 3H$, and $w/W = 1$ (Case 1) at plane $z/W = 0.1$.

Analyzing the velocity profiles, with the exception of the position $x = H$ at $z/W = 0.1$, as expected (the flows are mainly two-dimensional) no important variations are observed between the RSM simulations. However, it can be seen that the standard $k-\varepsilon$ model prescribes a different behavior of the velocity profiles close to the floor, which can be associated with the difficulty of this model in predicting secondary flows, mainly at line $x = H$.

Concerning the streamlines, see Fig. 8, note that the flow is almost vertical at $x = H$ independently of the room width. On the other hand, at $x = 2H$, when the width increases the flow is divided into two main circulations rotating in opposite senses.

Figure 9 illustrates the comparison between the numerical results for Case 4 obtained by standard $k-\varepsilon$ and RSM models and the experimental data for Case 2, in two lines of the room $x = H$ and $2H$ at planes $z/W = 0.5$ and $z/W = 0.1$. This figure shows that, in the central plane, the jet is not affected by the increase in the width of the room, but outside this region the numerical models predict higher gradients of velocity in the flow than it was observed in the experiments. In the plane, $z/W = 0.1$, one can note a decrease in the velocity and its gradients along with the height of the room, which can be attributed to a less important influence of the wall in the case of the largest room.

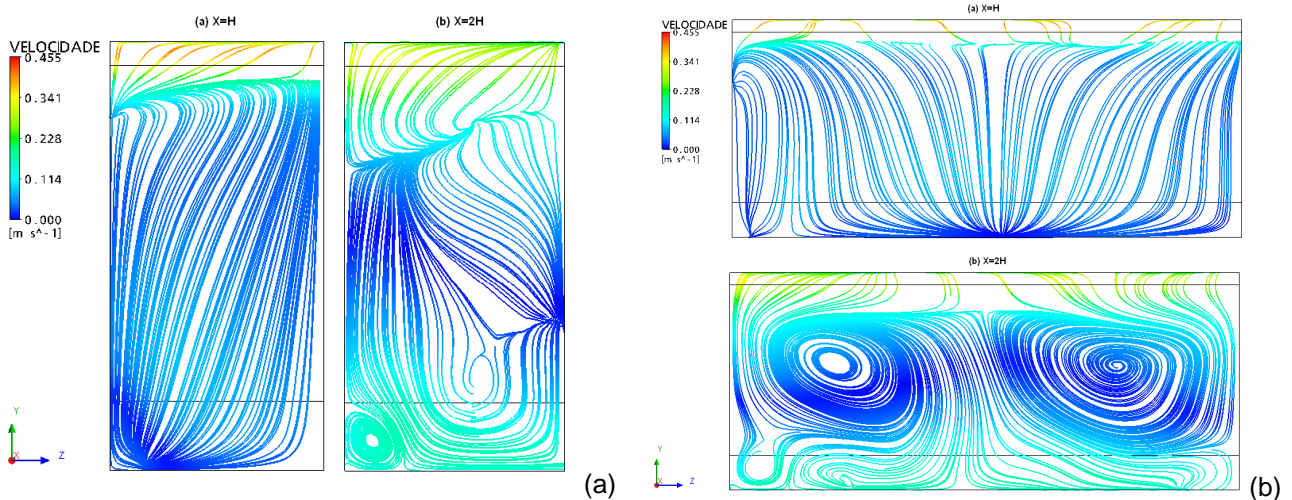


Figure 8. Comparison of streamlines predicted by the RSM model at planes $x = H$ and $x = 2H$, for (a) $W = 3H$ and $w/W = 1$ (Case 1), and (b) $W = 4.7H$ and $w/W = 1$ (Case 3).

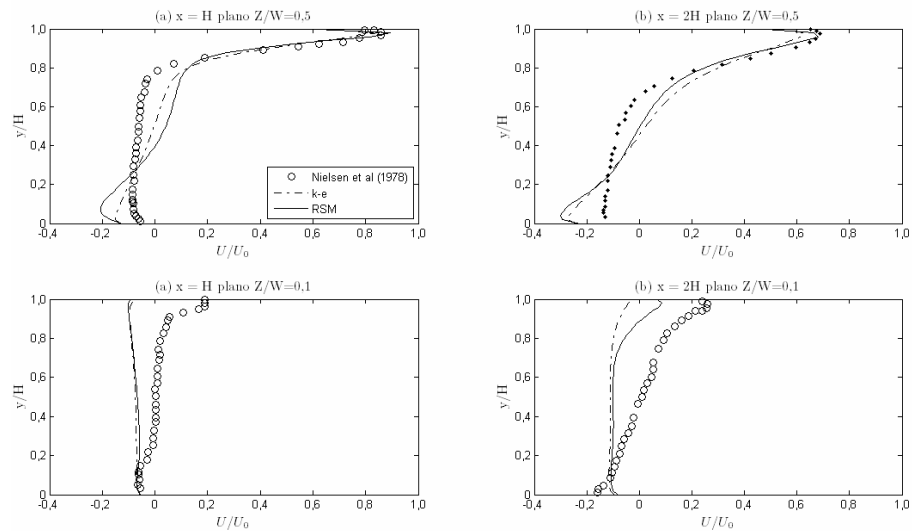


Figure 9. Comparison of dimensionless mean velocity profiles from standard $k-\epsilon$ and RSM models for $W = 4.7H$ and $w/W = 0.5$ (Case 4) to the experimental data for $W = 3H$ and $w/W = 0.5$ (Case 2) at $z/W = 0.5$ and 0.1 .

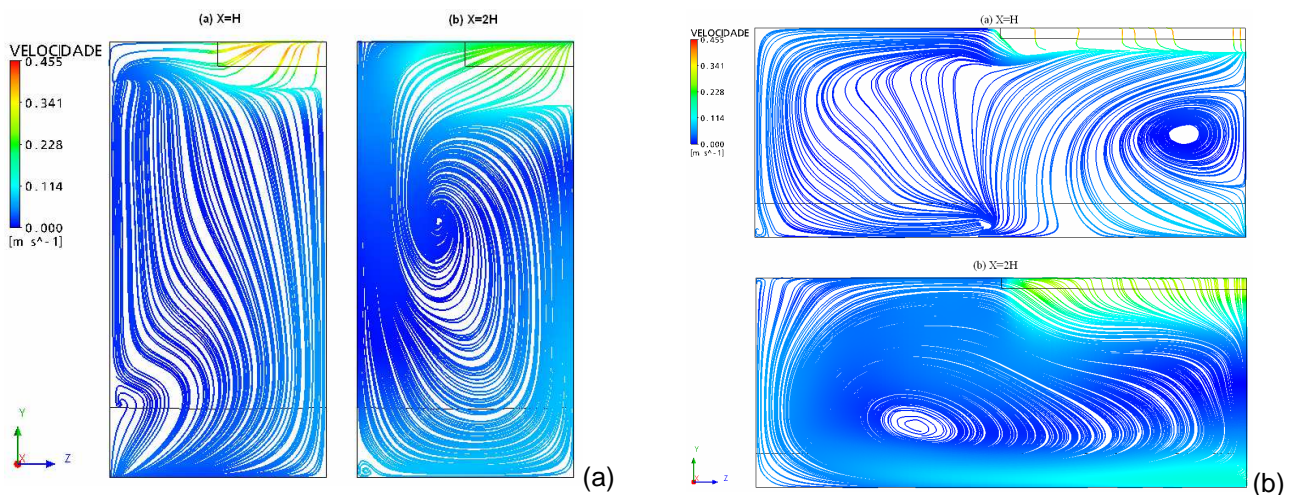


Figure 10. Comparison of streamlines predicted by the RSM model at planes $x = H$ and $x = 2H$, for (a) $W = 3H$ and $w/W = 0.5$ (Case 2), and (b) $W = 4.7H$ and $w/W = 0.5$ (Case 4).

The streamlines calculating by the RSM model for the cases whose the inlet slot width is half of the width of the room are compared in Fig. 10 at the positions $x = H$ and $x = 2H$. It can be seen in this figure that, in the plane $x = H$, the increase in the width of the room produces a recirculation below the inlet slot, and also displaces the main circulation at $x = 2H$ to the down left, reversing its direction of rotation when compared to the room with $W = 3H$.

5. CONCLUSIONS

In this work, the isotherm airflow regarding the Annex 20 test cell has been numerically studied using two turbulence models, the standard $k-\varepsilon$ and a RSM model, considering two aspect ratios of the room and two inlet slot widths. The comparative analysis between the predictions from the standard $k-\varepsilon$ and RSM models has shown that, in general, both models give similar velocity profiles. However, in terms of streamlines, the RSM model estimates more recirculations in the flow than the standard $k-\varepsilon$ model, as it has already been observed in the current literature.

When the room has been enlarged, important changes in the flow pattern have been noted, such as: two main circulations in a vertical plane at $x = 2H$ for the case whose inlet slot width is as large as the room; changing in the direction of the main circulation in the same plane for the other case ($w/W = 0.5$).

Concerning the width of the inlet slot, the velocities outside the central plane are reduced when the width of the inlet slot is reduced, and the flow pattern is strongly modified.

6. ACKNOWLEDGEMENTS

The authors would like to thank *Fundação Araucária* "Araucária Foundation for Scientific and Technological Development of Paraná" for the financial support to this work.

7. REFERENCES

- Chen, Q., 1996, "Prediction of room air motion by Reynolds-Stress models". *Building and Environment*. Vol. 31, pp. 233-244.
- Kolmogorov, A.N., 1942, "Equations of turbulent motion of an incompressible fluid". *Izvestia Acad. Sci., USSR; Phys.* Vol. 6, pp. 56-58.
- Launder, B. E.; Reece, G. J.; Rodin, W. 1975, "Progress in the developments of a Reynolds-stress turbulence closure". *Journal of Fluid Mechanics*, Vol. 68, pp. 537-566.
- Launder, B. E., Spalding, D. B., 1974, "The numerical computation of turbulent flows", *Comp. Meth. Appl. Mech. Energy*, Vol. 3, pp. 269-289.
- Lindner, G. A., Mendonça, K. C., Mariani, V. C., 2008, "Evaluating the performance of two eddy-viscosity turbulence models to predict mixed convection in a rectangular room", *Proceedings of the 12th Brazilian Congress of Thermal Sciences and Engineering*, pp. 1-10.
- Melikov, A.; Nielsen, P.V., 1989, "Local thermal discomfort due to draft and vertical temperature difference in rooms with displacement ventilation". *ASHRAE Transactions*, Vol. 96, pp. 1050-1057.
- Mora, L.; Gadgil, A. J.; Wurtz E., 2003, "Comparing zonal and CFD model predictions of isothermal indoor airflows to experimental data". *Indoor Air*, Vol. 13, pp. 77-85.
- Moureh, J., Flick, D., 2003, "Wall air-jet characteristics and airflow patterns within a slot ventilated enclosure", *International Journal of Thermal Sciences*, Vol. 42, pp. 703-711.
- Nielsen, P. V., 1990, "Specification of a two-dimensional test case", Technical report, International Energy Agency, Annex 20: Air Flow Pattern Within Buildings.
- Nielsen, P. V., Restivo, A., Whitelaw, J. H., 1978, "The velocity characteristics of ventilated rooms", *Journal of Fluid Engineering*, Vol. 100, pp. 291-298.
- Schälin, A., Nielsen, P. V., 2004, "Impact of turbulence anisotropy near walls in room airflow", *Indoor Air*, Vol. 14, pp. 159-168, 2004.
- Susin, R. M.; Lindner, G. A.; Mariani, V. C.; Mendonça, K. C., 2009, "Evaluating the influence of the width of inlet slot on the prediction of indoor airflow: comparison to experimental data". *Building and Environment*, Vol. 44, pp. 971-986.
- Prandtl, L., Wighardt, K., 1945, "Über ein neues formelsystem für die ausgebildete turbulenz", *Nachr. Akad. Wiss., Math.-Phys., Kl.*, 6.
- Reynolds, O., 1895, "On the dynamical theory of incompressible viscous fluids and the determination of the criterion", *Phil. Trans. Roy. Soc. London A*, Vol. 186, pp. 123-164.
- Versteeg, H. K. and Malalasekera, W., 1995, "An introduction to computational fluid dynamics", Longman Scientific & Technical, New York.
- Voigt, L.K., 2000, "Comparison of turbulence models for numerical calculation of airflow in an annex 20 room". Technical Report, Technical University of Denmark.

8. RESPONSIBILITY NOTICE

The authors Rafael Elias Mazzaro, Kátia Cordeiro Mendonça e Viviana Cocco Mariani are the only responsible for the printed material included in this paper.